RSC Advances

ROYAL SOCIETY OF CHEMISTRY

www.rsc.org/advances

Journal Name

Dynamic Article Links ►

Cite this: DOI: 10.1039/c0xx00000x

www.rsc.org/xxxxxx

ARTICLE TYPE

Biomimetic Multi-layered Hollow Chitosan-Tripolyphosphate Rod with Excellent Mechanical Performance

Jingyi Nie [a,b,§], Zhengke Wang [a,b,§,*], Kai Zhang [c] and Qiaoling Hu [a,b,*]

Received (in XXX, XXX) Xth XXXXXXXXX 20XX, Accepted Xth XXXXXXXXX 20XX

DOI: 10.1039/b000000x

In this work, chitosan-tripolyphosphate hydrogel and dry rod had been prepared, which possessed biomimetic features, *i.e.* multi-layered and hollow features. The ratio of internal to external diameter could be designed and controlled. The relationship between the biomimetic hierarchical structure and mechanical performance had also been explored in this research. The resulted rods with three-dimensional organized structure and excellent mechanical performance has great potential application in bone tissue engineering.

Introduction

Chitosan (CS), a polysaccharide obtained by the deacetylation of chitin, has received considerable attention for its intrinsic properties: biocompatibility, biodegradability, bacteriostatic effects and abundance in nature.[1-4] With applications pervading advanced industry and research, CS has been utilized in the preparation of various materials.[5-10] Hydrogel is a major branch and is a very important form of CS materials.[11, 12] CS hydrogel also provides a vital approach for the preparation of dry CS materials, such as scaffold and bone fracture internal fixation devices.[13-21] Therefore, the design of CS hydrogel is significant.[22, 23]

In the design of CS hydrogel materials, structures of natural materials had always been the source of inspiration. Biomimetic features could endow materials with excellent mechanical and functional performance. Multi-layered and hollow features are two successful examples. Multi-layered feature originated from natural structure like annual ring of trees and nacre shell, *etc.*[24, 25] This feature can improve the bending strength by stopping crack propagation.[26] Moreover, the hierarchical structure had applications in bio-related area, such as tissue engineering and controlled release of drugs.[27-30] The design of hollow rod was inspired from bamboo and straw, *etc*. Apart from mechanical benefits, the hollow feature enabled applications in blood vessel tissue engineering, spinal cord injury repair and nerve regeneration.[31-33]

In the design and fabrication of CS hydrogel, tripolyphosphate (TPPS) is a very popular ionic crosslinking agent because of its non-toxic property and mild gelation process.[34, 35] The incorporation of TPPS also introduced benefits in resulted chitosan-tripolyphosphate (CS-TPPS) composite materials, such as stability,[36, 37] antibacterial property,[38] and advantages in bone tissue engineering. CS-TPPS composite materials could improve cellular responses and supported biomineralization with phosphate as nucleation site.[39, 40] TPPS had been used for the preparation of crosslinked CS beads, gels, nanoparticles, and films.[41-43] CS-TPPS materials with layered structure were mainly fabricated by alternate processes, such as layer-by-layer self-assembly.[36, 38, 44] To our knowledge, the incorporation of TPPS in 3D CS rod with organized structure had not been reported. In this work, multi-layered hollow CS-TPPS hydrogel and dry rod had been prepared by a very simple process, and the relationship between the multi-layered hollow structure and mechanical performance had also been explored in the following section.

Experimental section

1.Materials

CS was purchased from Zhejiang Gold Shell Pharmaceutical Co. Ltd. The average viscosity molecular weight ($M\eta$) of CS was 5.63×10^5 Da, and degree of deacetylation (DD) was 91%. Sodium tripolyphosphate was purchased from Sinopharm Chemical Reagent Co., Ltd.. The other chemical reagents used in the work were all of analytical reagent grade.

2.Preparation of multi-layered hollow CS-TPPS rod

CS powder was dissolved in 2 vol.% acetic acid aqueous solution to prepare CS solution (5 wt.%). A cylindrical semipermeable membrane was used as mold. Subsequently, the cylindrical mold was filled with CS solution, followed by precipitation in 5% (w/v) NaOH aqueous solution to form CS gel rod. CS gel rods were washed with deionized water repeatedly to remove OH^-. The pH of CS gel rods was modulated to be 6.5 by sulphuric acid and then immersed in TPPS aqueous solution with desired concentration for 12 h. The resulted rods were washed with deionized water repeatedly to remove the salt. Dry CS-TPPS rods were prepared by air-drying in an oven at 60 °C for 24 h. For the preparation of pure dry CS rods, CS gel rods were washed with deionized water repeatedly to be neutral and then dried.

3.Relationship of gel thickness and precipitation time.

CS solution (5 wt.%) was filled in a single opening glass tub

and immersed in 5% (w/v) NaOH aqueous solution. The thickness of precipitated CS gel was observed and recorded with time.

4.Scanning electron microscopy (SEM)

The fracture surface of CS rod was observed by SEM. Samples were air-dried in oven at 60 ˚C for 6 h to remove the remaining moisture, and then gold-sprayed for conductance. HITACHI S-4800 SEM was used in this study.

5.Fourier transform infrared spectroscopy (FTIR)

FTIR spectra of samples were obtained with a VECTOR 22 spectrophotometer (Bruker, Germany) in the wavenumber range of 2000-800 cm^{-1}.

6.Thermogravimetric-derivative thermogravimetry (TG-DTG)

Thermal analyses were carried out by a Pyris-6 Thermo Analyse (PerkinElmer). Samples were heated from 50 to 600 ˚C at a heating rate of 20 ˚C/min under a constant flow of nitrogen (40 ml/min).

7. Mechanical properties

The bending strength and modulus of CS or CS-TPPS rods were tested by three point bending test on a universal mechanical testing apparatus (Shenzhen Reger Company, China). The span length was 40 mm and loading rate was 2 mm/min, and the ultimate bending strength (σ_b) and bending modulus (E_b) of the rods were calculated according to Eqs. (1) and (2), respectively[45, 46]

$$\sigma_b = \frac{8F_{max}L}{\pi d^3(1-\alpha^4)} \quad (1)$$

$$E_b = \frac{4L^3}{3\pi d^4(1-\alpha^4)}\frac{\Delta F}{\Delta l}\frac{1}{1000} \quad (2)$$

where F_{max} is the maximum bending force recorded (N), L the support span (mm), d the external diameter of the rod (mm), α the ratio of internal to external diameter, and $\Delta F/\Delta l$ the slope of the force-deflection curve of the initial linear section (N/mm).

Results and Discussion

1. Formation of multi-layered and hollow structure

Multi-layered hollow CS-TPPS rod had regular shape and smooth surfaces (Fig.1). The hollow feature can be observed in Fig.1b to Fig.1d. Furthermore, the hollow rod possessed multi-layered feature, and some of the layers were visible to the naked eye (Fig.1b and Fig.1c). During the drying process, swollen macromolecules started to shrink. This effect contributed to more compact structure. As a result, multi-layers in dry hollow rod cannot be observed directly by visual inspection.

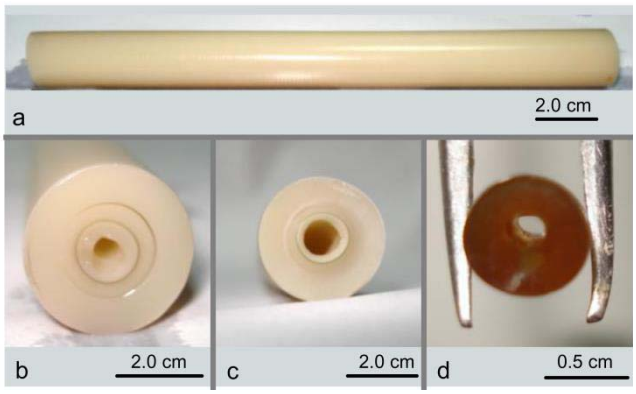

Fig. 1 Digital photographs of multi-layered hollow CS-TPPS rod. (a) overall view of hydrogel rod; (b-d) cross section of rod: (b) hydrogel rod, (c) hydrogel rod after drying for 8 h, (d) dried rod.

CS became soluble in acetic acid aqueous solution because of the protonation of $-NH_2$ groups.[47-50] And the CS solution could be turned into hydrogel when it came in contact with alkali. The gelation process of this system possessed a layer-wise characteristic.[51] As shown in Fig.2a, when OH^- diffused into CS solution along one-dimensional direction, the thickness of hydrogel increased with time. The resulted hydrogel had multi-layers, which were parallel to the equipotential surface of $c(OH^-)$ (Fig.2b). The formation of layers could be explained by the Liesegang ring phenomenon, caused by the encounter of an inner and an outer electrolytes and their periodical precipitation in the supporting medium. In this system, CS played dual roles of the inner electrolyte and the supporting medium.

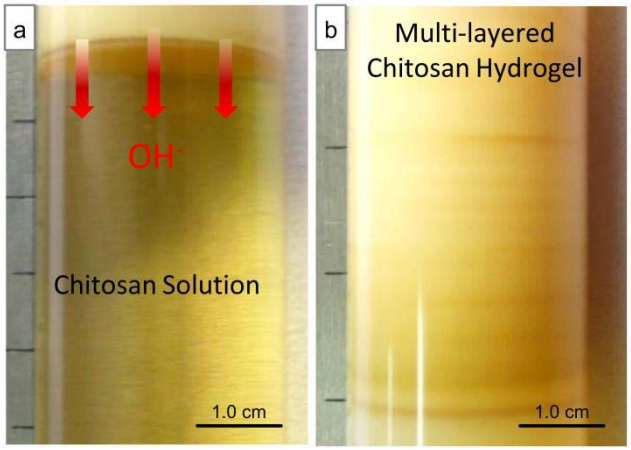

Fig. 2 Layer-wise precipitation of CS solution: (a) diffusion direction of OH^- to chitosan solution, (b) multi-layered chitosan hydrogel.

The design and construction of multi-layers in the rod was demonstrated below and schematically shown in Scheme 1. Diffusion direction of OH^- was arranged to be three-dimensional, which was from the outer surface of semipermeable membrane to the central axis. The equipotential surfaces of $c(OH^-)$ were cylindrical, and the resulted hydrogel layers were in the form of concentric cylinders, which formed multi-layered rod.

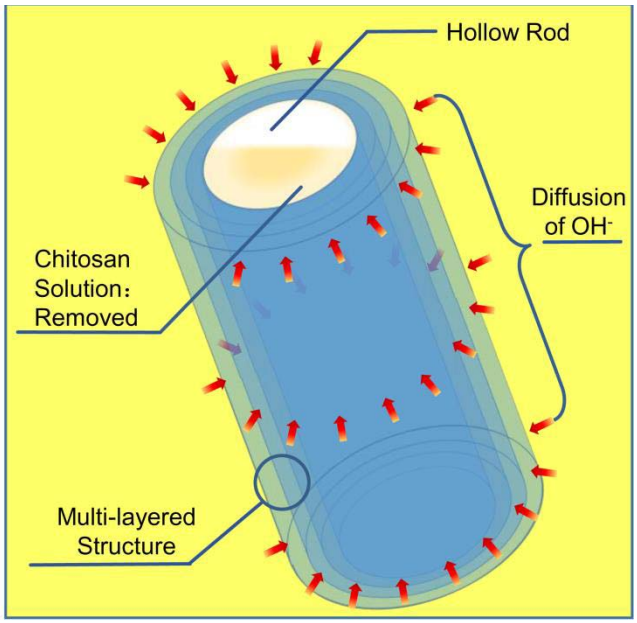

Scheme 1 Preparation and structural features of multi-layered hollow CS-TPPS rod.

Multi-layered structure could be observed in pure CS rod and CS-TPPS rod by SEM (Fig.3a and Fig.3b). TPPS contains P-O^- moiety and could create ionic crosslinking points with protonated amino moiety -NH^{3+}. But when CS hydrogel was neutral, the proportion of -NH^{3+} was low, and cannot form effective crosslinks. On the other hand, lower pH could increase -NH^{3+} and combination with TPPS, however it may also destroy the multi-layered structure. So proper pH was selected to make sure that CS hydrogel was only slightly swollen while being reactive with TPPS. [52] Results showed that this method did not affect the shape of hydrogel, and multi-layered feature was successfully maintained in CS-TPPS rod (Fig.3b). And the interaction between CS and TPPS was discussed in the next section.

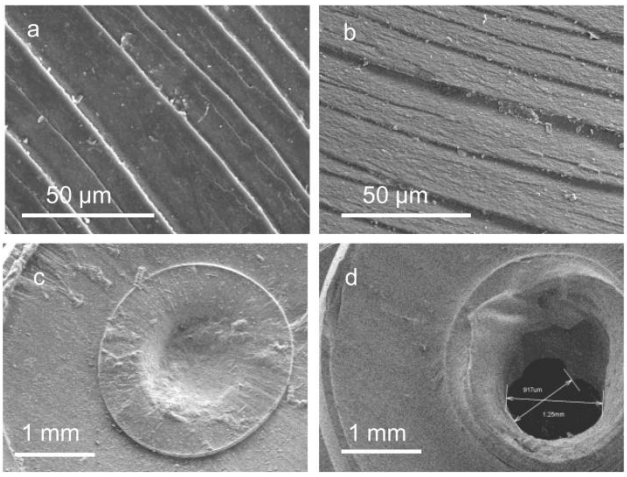

Fig. 3 SEM images of CS rods: (a-b) multi-layered structure of CS and CS-TPPS rods, respectively; (c-d) cross section view of central area in solid and hollow CS-TPPS rods, respectively.

The hollow feature of CS-TPPS rod was constructed by utilizing the layer-wise gelation process, *i.e.* the relationship between gel thickness and time. The thickness of gel did not grow linearly with time all along (Fig.4). In the first hour, gel thickness increased from 0 to 7 mm. In first 7 hours, the increasing rate of gel thickness declined gradually, and the average rate was 2.71 mm/h. The increasing rate of gel thickness reached a constant (0.33 mm/h) after 7 h. This was because the increasing rate of gel thickness was determined by the diffusion rate of OH^- to the gel-sol interface. When the thickness of gel was small (<10 mm), the $c(OH^-)$ in the gel had not reached equilibrium with that in the coagulation bath. So the coagulation bath was the major source of OH^-. [51] Thus the thickness of gel had significant effect on the diffusion of OH^-. With longer precipitation time, the thickness of gel increased and $c(OH^-)$ in the upper part of gel had reached the value of coagulation bath.[53] The upper part of gel gradually became the source of OH^- for the gel-sol interface. As a result, the distance between coagulation bath and the interface had little impact on the increasing rate of gel thickness.

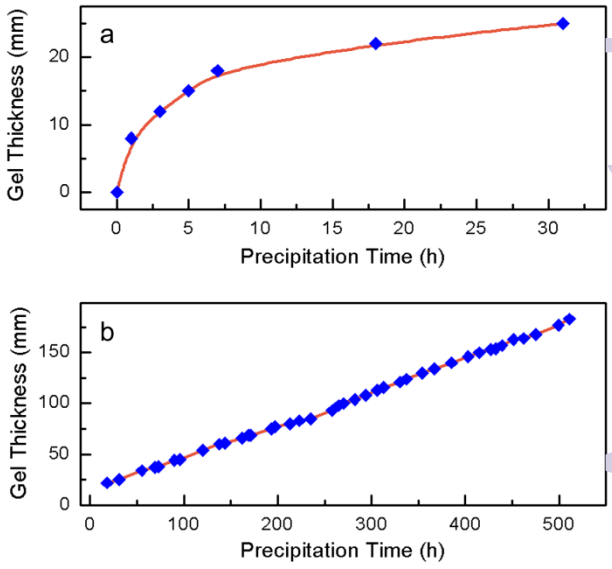

Fig. 4 Gel thickness for different precipitation time: (a) 0-30 h, (b) 30-500 h.

The understanding of relationship between gel thickness and precipitation time was crucial in the design of hollow structure. When immersed in the NaOH coagulation bath for sufficient time, all CS solution finished precipitation. There was no space in the central area of the rod (Fig.3c). However, if the precipitation was terminated before gel thickness reached the radius of cylindrical mold, hollow rod was formed (Fig.3d). The internal diameter of hollow rod was the difference between external radius and gel thickness. Thus by controlling precipitation time, the ratio of internal diameter to external diameter (α) could be modulated.

2. Determination of ionic crosslinks between CS and TPPS

FTIR spectra of CS and CS-TPPS rods had been analysed to determine the interaction between CS and TPPS (Fig.5a). The absorption band in the high wavenumber region (>3000 cm^{-1}) corresponded to the -O-H and -N-H stretching vibrations of CS which was an overlapped broadband. So the analyze focused on the region of 2000-800 cm^{-1}. For pure CS rod, the characteristic absorption peaks of CS were observed: 1655 cm^{-1} ($\tilde{V}_{N\text{-}H,}$ -CO-N

amide band Ⅰ), 1598cm^{-1} ($\delta_{N\text{-}H}$, amide band Ⅱ), 1423 cm^{-1} and 1378 cm^{-1} ($\tilde{V}_{N\text{-}H}$, amide band Ⅲ), 1155 cm^{-1} ($\tilde{V}_{C\text{-}O}$), 1074cm^{-1} ($\tilde{V}_{C\text{-}O}$, -CH-OH), and 1030 cm^{-1}($\tilde{V}_{C\text{-}O}$, -CH_2-OH). For CS-TPPS rod, the characteristic absorption peaks of TPPS were observed at 1210-1082 cm^{-1} ($\tilde{V}_{P\text{-}O}$ $\tilde{V}_{P=O}$) and 879 cm^{-1}($\delta_{P\text{-}O}$). Moreover, the characteristic absorption bands of CS between 1155 cm^{-1} to 1082 cm^{-1} merged with absorption peaks of TPPS. These confirmed the successful incorporation of TPPS in the rod. In addition, stretching frequency at 1655 cm^{-1} and 1598 cm^{-1} merged to be one peak with enhanced intensity, indicating that reaction had taken place on the amino groups. Altogether the FTIR spectra indicated that ionic crosslinks had taken place between protonated amine moiety -NH^{3+} of CS and P-O^- moiety of TPPS.

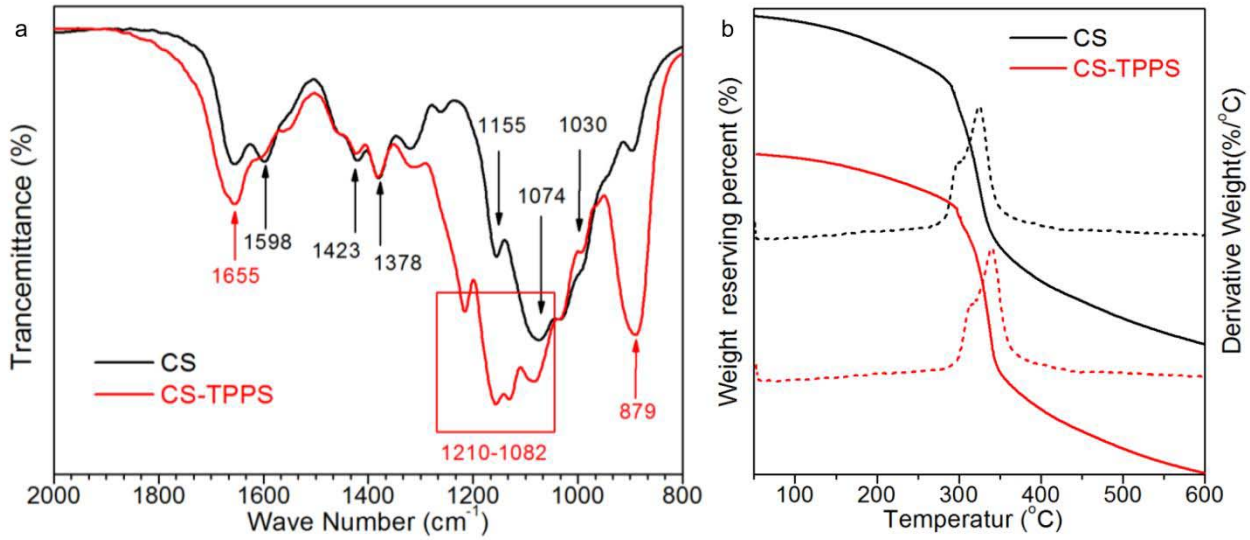

Fig. 5 FTIR spectra and TG/DTG curves of CS and CS-TPPS rod.

To demonstrate the reaction between CS and TPPS, the thermal analysis on CS and CS-TPPS rods had been conducted. The TG and DTG curves of CS and CS-TPPS rods were shown in Fig.5b. The major weight losses observed at 250-450°C were attributed to the decomposition of the CS. Compared with CS rod, the TG curves of CS-TPPS rod shifted to higher temperature. As can be seen from the DTG curves, peaks of the maximum decomposition rate were observed at 324 and 338°C for CS and CS-TPPS rods, respectively. This fact provided an additional evidence for the formation of ionic crosslinks. [54]

3. The relationship between biomimetic structure and mechanical performance

The mechanical properties of CS-TPPS multi-layered hollow rods had been tested. The influence of TPPS was demonstrated in Fig.6a. Results showed that for samples with α=0.17, the bending strength was in the range of 108.0-154.8 MPa, and the bending modulus was in the range of 4.1~5.6 GPa. These values were higher than that of pure CS rods. Moreover, with the increase of *c*(TPPS) in crosslinking bath, the bending strength and modulus both increased. It can be concluded that the incorporation of TPPS enhanced the mechanical performance. Ionic crosslinks formed between CS and TPPS in addition to inter-/intro-molecular hydrogen bonds, and improved the mechanical performance on molecular level.[55]

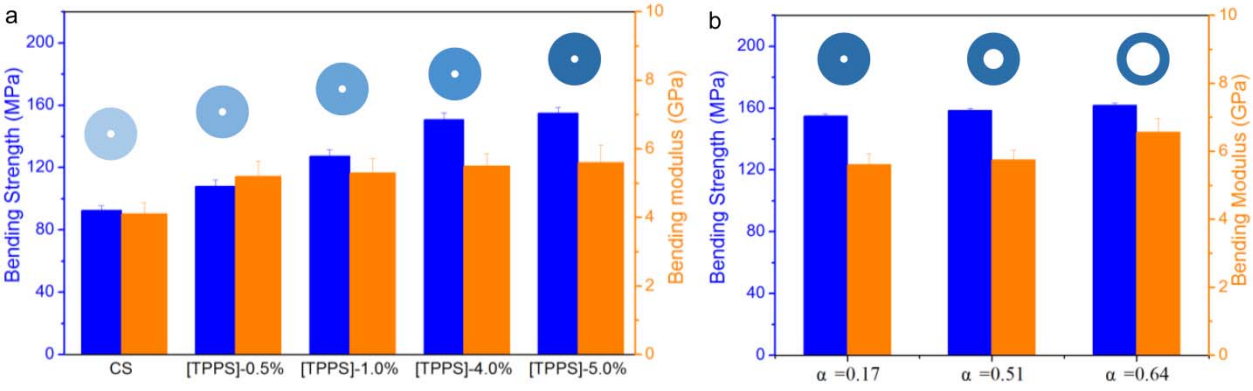

Fig. 6 Mechanical properties of CS-TPPS multi-layered hollow rods. (a) the influence of the concentration of TPPS in cross-linking bath, α=0.17, (b) the influence of the ratio of internal diameter to external diameter, *c*(TPPS)=5% in cross-linking bath; All samples had the same external diameter and length.

The influence of structural characteristics was also studied. The influence of ratio of internal to external diameter (α) was

demonstrated in Fig.6b.The bending strength and modulus of multi-layered hollow rod showed a tendency of increase with the rise of α. The shape of cross section is very important for the mechanical properties of materials. For solid and hollow rod that had same area of cross section, their section moduli were different. Section modulus (W_Z) is critical in bending behaviour of rod materials, and higher value of this parameter is favoured for the improvement of bending strength.[56] The section modulus ratio of solid and hollow rod is:

$$\frac{W_{Z,\text{solid}}}{W_{Z,\text{hollow}}} = \frac{\sqrt{1-\alpha^2}}{1+\alpha^2} \leq 1 \quad (3)$$

This indicated hollow rod always had higher section modulus than solid rod, which led to higher bending strength. However, discussion above was based on the premise that the two kinds of rods had same area of cross section, *i.e.* the same mass for certain length. If hollow and solid rods had the same external diameter, the advantage of hollow feature was in conflict with the decrease of effective cross section area (Scheme 2). The ratio of bending modulus (σ_b) of hollow and solid rods was demonstrated in Eqs.(4):

$$\frac{\sigma_{b,hollow}}{\sigma_{b,solid}} = \frac{F_{max,hollow}}{F_{max,solid}} \cdot \frac{1}{(1-\alpha^4)} \quad (4)$$

Although the increase of α is favoured in the view of cross section shape, the maximum bending force (F_{max}) may decrease due to reduced cross section area. This situation resembles the decay of trunks, which results increased risk of failure.[56] According to analysis above, the increase of α was not favoured when the external diameter was fixed. However, it was noteworthy that the rise of α was actually advantageous as demonstrated in Fig.6b. If the mass of rod was also taken into consideration, the advantage was more evident as demonstrated by Eqs.(5).

$$\frac{\sigma'_{b,hollow}/m_{hollow}}{\sigma'_{b,solid}/m_{solid}} = \frac{\sigma_{b,hollow}}{\sigma_{b,solid}} \cdot \frac{1}{(1-\alpha^2)} \quad (5)$$

This phenomenon had two contributing factors: 1) the compression caused by drying stress and 2) the gradient of modulus in CS hydrogel. 1) During the drying process, there existed a difference of water content between the surface and the interior part of rod, thus created drying stress towards the interior part.[57] The radial drying stress was perpendicular to the cylindrical surface of rod.[58] Since hollow rod had both external and internal surfaces, the radial stress created a compression effect (Scheme 2b), and led to more compact structure. 2) CS hydrogel prepared by precipitation from acidic solution was not homogeneous material. The modulus of hydrogel decreased with the increase of distance to the primary hydrogel layer.[51] For rod material, the primary hydrogel layer corresponded to the external surface of cylinder, thus the centre was the most distant point. So the modulus of hydrogel decreased along the radial direction as shown in Scheme 2c. The average modulus of hydrogel in 0-10 mm distance range was approximately twice the value of that in 10-20 mm distance range.[51] In the case of the present work, although the area of cross section was decreased, hydrogel near the external surface was preserved, which had higher modulus than the average modulus of solid rod.

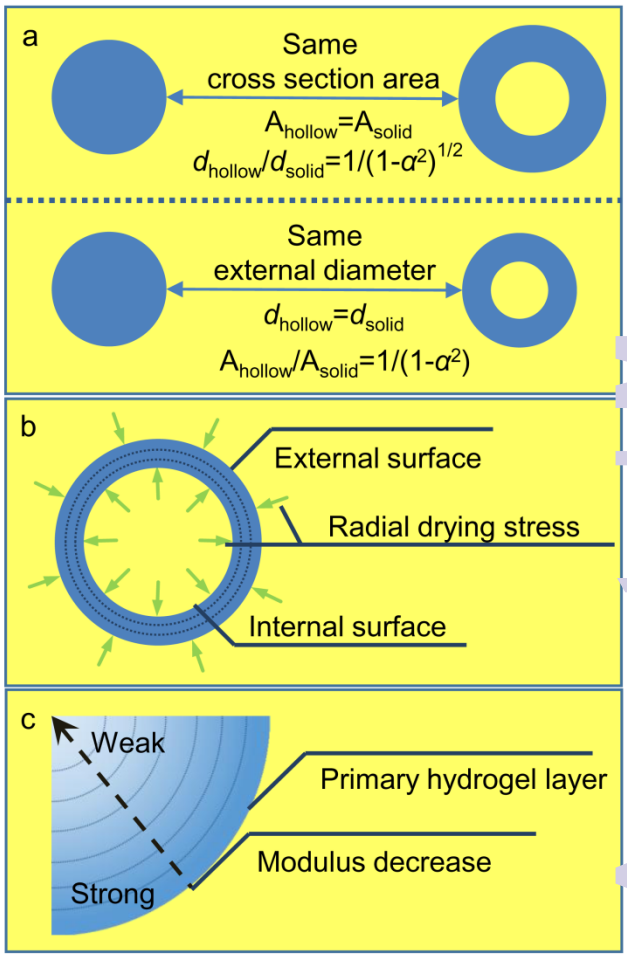

Scheme 2 The influence of structural characteristics on chitosan rod. (a) relationship between solid and hollow rods; (b)compression of drying stress in CS-TPPS multi-layered hollow rod; (c) modulus gradient in CS hydrogel rod.

Conclusion

In summary, a CS-TPPS rod with biomimetic multi-layered and hollow features had been prepared. Moreover these features were achieved as well as excellent mechanical performance. The preparation was simple and based on the controlled precipitation of CS solution. The external and internal diameters could both be designed and controlled. TPPS had been successfully introduced into the 3D CS rod via ionic crosslinks. The inclusion of TPPS improved the mechanical performance while endowed properties such as benefits in bone tissue engineering. The multi-layered hollow features greatly improved the mechanical performance of CS-TPPS rods. This material had potential applications in bio-related fields, especially the case in which mechanical performance and sophisticated 3D structure are both required .

Acknowledgements

This work was financially supported by National Natural Science Foundation of China (Nos. 21104067, 21274127, 21374099 and 51473144), and Key Basic Research Development Plan (973 Program) of China (Nos. 2009CB930104 and 2011CB606203).

Acknowledgements

This work was financially supported by the National Natural Science Foundation of China (Nos. 21104067, 21274127, 21374099 and 51473144), the Key Basic Research Development Plan (973 Program) of China (Nos. 2009CB930104 and 2011CB606203), the Science and Technology Project of Zhoushan City (No. 2011C12054), and the Grand Science and Technology Innovative Research Team of Zhejiang Province (No. 2013TD02).

Author contributions

§J.Y.Nie and Z.K.Wang contributed equally to this work.

Notes and references

[a] *MOE Key Laboratory of Macromolecular Synthesis and Functionalization, Department of Polymer Science and Engineering, Zhejiang University, Hangzhou 310027, China. Email: wangzk@zju.edu.cn; huql@zju.edu.cn.*
[b] *Joint Laboratory for Adsorption and Separation Materials of Zhejiang University-Zhejiang Tobacco Industry Co. Ltd, Zhejiang University, Hangzhou 310027, China*
[c] *Affiliated Stomatology Hospital of Medicine College, Zhejiang University, Hangzhou 310006, China*

1 M. Rinaudo, *Prog. Polym. Sci.*, 2006, **31**, 603-632.
2 L. Chen, C. Y. Tang, N. Y. Ning, C. Y. Wang, Q. Fu and Q. Zhang, *Chin. J. Polym. Sci.*, 2009, **27**, 739-746.
3 J. W. Jia, Z. K. Wang, W. T. Lu, L. Yang, Q. W. Wu, W. Qin, Q. L. Hu and B. Z. Tang, *J. Mater. Chem. B*, 2014, **2**, 8406-8411.
4 K. Zhang, M. Zhao, L. Cai, Z. K. Wang, Y. F. Sun and Q. L. Hu, *Chin. J. Polym. Sci.*, 2010, **28**, 555-561.
5 M. Li, Y. N. Hong, Z. K. Wang, S. J. Chen, M. Gao, R. T. K. Kwok, W. Qin, J. W. Y. Lam, Q. C. Zheng and B. Z. Tang, *Macromol. Rapid Commun.*, 2013, **34**, 767-771.
6 Y. L. Li, P. Y. Zhuang, Y. F. Zhang, Z. K. Wang and Q. L. Hu, *Mater. Lett.*, 2012, **84**, 73-76.
7 Y. F. Sun, Y. L. Li, J. Y. Nie, Z. K. Wang and Q. L. Hu, *Chem. Lett.*, 2013, **42**, 838-840.
8 Z. K. Wang, S. J. Chen, J. W. Y. Lam, W. Qin, R. T. K. Kwok, N. Xie, Q. L. Hu and B. Z. Tang, *J. Am. Chem. Soc.*, 2013, **135**, 8238-8245.
9 K. Zhang, Z. K. Wang, Y. L. Li, Z. Q. Jiang, Q. L. Hu, M. Y. Liu and Q. X. Zhao, *Carbohydr. Polym.*, 2013, **92**, 662-667.
10 K. Zhang, P. Y. Zhuang, Z. K. Wang, Y. L. Li, Z. Q. Jiang, Q. L. Hu, M. Y. Liu and Q. X. Zhao, *Carbohydr. Polym.*, 2012, **90**, 1515-1521.
11 A. El Kadib, M. Bousmina and D. Brunel, *J. Nanosci. Nanotechnol.*, 2014, **14**, 308-331.
12 S. D. Ray, *Acta Pol. Pharm.*, 2011, **68**, 619-622.
13 T. S. Anirudhan and A. M. Mohan, *RSC Adv.*, 2014, **4**, 12109-12118.
14 H. Liu and C. Y. Wang, *RSC Adv.*, 2014, **4**, 3864-3872.
15 X. M. Pu, Z. Z. Sun, Z. Q. Hou, Y. Yang, Q. Q. Yao and Q. Q. Zhang, *J. Biomed.Mater. Res., Part B*, 2012, **100B**, 1179-1189.
16 J. Z. Zhang, J. Y. Nie, Q. R. Zhang, Y. L. Li, Z. K. Wang and Q. L. Hu, *J. Biomater. Sci., Polym. Ed.*, 2014, **25**, 61-74.
17 J. H. Ke, Z. K. Wang, Y. Z. Li, Q. L. Hu and J. Feng, *Chin. J. Polym. Sci.*, 2012, **30**, 436-442.
18 X. Wang, Y. Gao, H. Zhao, X.-Q. Liu, Z. Wang, A. Qin, Q. Hu, J. Z. Sun and B. Z. Tang, *Polym. Chem.*, 2014, **5**, 6216-6224.
19 Z. K. Wang and Q. L. Hu, *Biomed. Mater.* , 2010, **5**, 045007.
20 Z. K. Wang, Q. L. Hu, X. G. Dai, H. Wu, Y. X. Wang and J. C. Shen, *Polym. Compos.*, 2009, **30**, 1517-1522.
21 Z. K. Wang, H. Zhao, L. Fan, J. Lin, P. Y. Zhuang, W. Z. Yuan, Q. L. Hu, J. Z. Sun and B. Z. Tang, *Carbohydr. Polym.*, 2011, **84**, 1126-1132.
22 J. Berger, M. Reist, J. M. Mayer, O. Felt and R. Gurny, *Eur. J. Pharm. Biopharm.*, 2004, **57**, 35-52.
23 J. Berger, M. Reist, J. M. Mayer, O. Felt, N. A. Peppas and R. Gurny, *Eur. J. Pharm. Biopharm.*, 2004, **57**, 19-34.
24 M. Suzuki and H. Nagasawa, *Can. J. Zool.*, 2013, **91**, 349-366.
25 S. S. Wang, Y. Q. Shu, B. L. Liang, L. C. Gao, M. Gao, P. G. Yin and L. Guo, *Chin. J. Polym. Sci.*, 2014, **32**, 675-680.
26 Z. K. Wang, Q. L. Hu and Y. X. Wang, *Sci. China: Chem.*, 2011, **54**, 380-384.
27 K. Lee, G. Jin, C. H. Jang, W. K. Jung and G. Kim, *J. Mater. Chem. B*, 2013, **1**, 5831-5841.
28 T. J. Levingstone, A. Matsiko, G. R. Dickson, F. J. O'Brien and J. P. Gleeson, *Acta Biomater.*, 2014, **10**, 1996-2004.
29 B. B. Hsu, S. R. Hagerman, K. Jamieson, J. Veselinovic, N. O'Neill, E. Holler, J. Y. Ljubimova and P. T. Hammond, *Biomacromolecules*, 2014, **15**, 2049-2057.
30 B. Mu, P. Liu, Y. Dong, C. Y. Lu and X. L. Wu, *J. Polym. Sci., Part A*, 2010, **48**, 3135-3144.
31 K. Haastert-Talini, S. Geuna, L. B. Dahlin, C. Meyer, L. Stenberg, T. Freier, C. Heimann, C. Barwig, L. F. V. Pinto, S. Raimondo, G. Gambarotta, S. R. Samy, N. Sousa, A. J. Salgado, A. Ratzka, S. Wrobel and C. Grothe, *Biomaterials*, 2013, **34**, 9886-9904.
32 X. G. Li, Z. Y. Yang, A. F. Zhang, T. L. Wang and W. C. Chen, *Biomaterials*, 2009, **30**, 1121-1132.
33 J. R. Zhang, L. K. Yi and J. C. Zhang, *Neural Regeneration Res.*, 2010, **5**, 668-672.
34 P. Sun, P. Li, Y. M. Li, Q. Wei and L. H. Tian, *J. Biomed.Mater. Res., Part B*, 2011, **97B**, 175-183.
35 Y. L. Hu, W. Qi, F. Han, J. Z. Shao and J. Q. Gao, *Int. J. Nanomed.* , 2011, **6**, 3351-3359.
36 S. W. Ali, M. Joshi and S. Rajendran, *Aatcc Review*, 2011, **11**, 49-55.
37 P. Sacco, M. Borgogna, A. Travan, E. Marsich, S. Paoletti, F. Asaro, M. Grassi and I. Donati, *Biomacromolecules*, 2014, **15**, 3396-3405.
38 A. R. Shirvan, N. H. Nejad and A. Bashari, *Fibers Polym.* , 2014, **15**, 1908-1914.
39 M. Kucharska, K. Walenko, B. Butruk, T. Brynk, M. Heljak and T. Ciach, *Mater. Lett.*, 2010, **64**, 1059-1062.
40 F. Pati, H. Kalita, B. Adhikari and S. Dhara, *J. Biomed. Mater. Res., Part A*, 2013, **101**, 2526-2537.
41 L. Jin, X. Zeng, M. Liu and N. Y. He, *Sci. Adv. Mater.*, 2013, **5**, 2053-2057.
42 A. Rampino, M. Borgogna, P. Blasi, B. Bellich and A. Cesaro, *Int. J. Pharm.*, 2013, **455**, 219-228.
43 A. Anitha, N. Deepa, K. P. Chennazhi, S. V. Nair, H. Tamura and R. Jayakumar, *Carbohydr. Polym.*, 2011, **83**, 66-73.
44 S. Shenvi, A. F. Ismail and A. M. Isloor, *Desalination*, 2014, **344**, 90-96.
45 A. Saikku-Backstrom, R. M. Tulamo, T. Pohjonen, P. Tormala, J. E. Raiha and P. Rokkanen, *J. Mater. Sci.: Mater. Med.*, 1999, **10**, 1-8.
46 K. Shen and Q. L. Hu, *Mater. Lett.*, 2011, **65**, 1503-1505.
47 Z. K. Wang, Q. L. Hu and L. Cai, *Chin. J. Polym. Sci.*, 2010, **28**, 801-806.
48 C. K. S. Pillai, W. Paul and C. P. Sharma, *Prog. Polym. Sci.*, 2009, **34**, 641-678.
49 Z. K. Wang and Q. L. Hu, *Acta Phys. Chim. Sin.* , 2010, **26**, 2053-2056.
50 Z. K. Wang, Q. L. Hu and L. Cai, *Int. J. Polym. Sci.*, 2010, **2010,** 369759.
51 J. Nie, W. Lu, J. Ma, L. Yang, Z. Wang, A. Qin and Q. Hu, *Sci. Rep.*, 2015, **5**, 7635
52 M. Rinaudo, G. Pavlov and J. Desbrieres, *Polymer*, 1999, **40**, 7029-7032.
53 H. Zhang and W. Davison, *Anal. Chim. Acta*, 1999, **398**, 329-340.
54 F. S. Pereira, D. L. D. Agostini, A. E. Job and E. R. P. Gonzalez, *J. Therm. Anal. Calorim.*, 2013, **114**, 321-327.

55 A. Aryaei, A. H. Jayatissa and A. C. Jayasuriya, *J. Mech. Behav. Biomed. Mater.* , 2012, **5**, 82-89.
56 A. Koizumi and T. Hirai, *J. Wood Sci.*, 2006, **52**, 213-219.
57 B. Clair, *Holzforschung*, 2012, **66**, 349-353.
58 W. Cheng, T. Morooka, Q. Wu and Y. Liu, *Forest Prod. J.*, 2007, **57**, 39-43.